Preprints of the 21st IFAC World Congress (Virtual)
Berlin, Germany, July 12-17, 2020

Power Loss Analysis of Bidirectional ACFC-SR Based Active Cell Balancing System ⋆

Kai Shi *, **Truong Q. Dinh** *, **James Marco** *

* *Warwick Manufacturing Group (WMG), The University of Warwick, Coventry, CV4 7AL UK (Kai.Shi@warwick.ac.uk, T.Dinh@warwick.ac.uk, James.Marco@warwick.ac.uk).*

Abstract: With the expansion of the number of electric vehicles (EV) over the world, the research on the battery and the battery management system (BMS) have become more popular. The active balancing, which is working as an advanced function in the modern BMS, has attracted researchers' attention to enhance battery system performance and prolong the battery pack life via integration of specially designed power electronic circuit with proper control and optimisation strategies in the BMS. This paper develops the power-loss and efficiency models of the bidirectional active clamp forward converter with synchronous rectifier (ACFC-SR) based active cell balancing system. The developed models can be involved in the power loss analysis of the active cell balancing system to underpin the energy efficiency performance evaluation and the balancing control system design of active balancing systems. The optimal balancing current with which the converter would operate at the maximum efficiency point can be obtained via the developed efficiency model. A case study is also included to illustrate the efficiency performance of the active balancing system.

Keywords: active cell balancing, active clamp forward converter, power loss analysis

1. INTRODUCTION

Lithium-ion battery packs have been widely used in electric vehicles because of their high energy density. To meet the requirement of high voltage output, the lithium-ion battery cells need to be connected in series (see Cordoba-Arenas et al. (2015)). The performance of a lithium-ion battery system with the series topology is affected by cell imbalance due to the manufacturing inconsistencies and different operating conditions among the cells. The available energy of a battery pack with imbalanced cells is lower than its total energy and it causes a reduction in real energy capacity of the battery pack (see Lee et al. (2015)). One of the main functions of the modern battery management system (BMS) is to maintain balanced cells in the battery pack. With cell balancing technology applied in the BMS, the charge stored within each cell can be equalised and the imbalances can be eliminated such that a maximum available energy capacity of the battery pack can be obtained.

The passive and active balancing are two main categories of cell balancing methods. The passive balancing methods can be applied during the charging process of a battery pack to ensure that every cell is fully charged (see Kutkut and Divan (1996)). The active balancing methods balance the cells via cell energy redistribution, which is more energy-efficient than the passive balancing methods that dissipate excessive cell energy to resistors and the active methods are more suitable to get involved in both charging and discharging operations (see Daowd et al. (2011)). An active balancing system circuit that employs a bidirectional ACFC-SR is presented in Fig.1, which has been used by Texas Instruments in their active balancing product (e.g. TI EM1402 active balancing board). The energy redistribution among cells is achieved via exchanging the energy between the battery cells and an auxiliary power source. The similar topology has been mentioned and discussed in the work of Hannan et al. (2017) and Daowd et al. (2011). The bidirectional ACFC-SR is shared by all the cells connected to the balancing system and only one cell can be connected to it each time via the switching matrix to be charged or discharged. The magnitude and the direction of the balancing current can be controlled by controlling the inductor current of the bidirectional ACFC-SR.

Although the active balancing circuits result in a less energy loss compared to a passive one, the switching devices, the passive components, the power electronics driver circuit, and the control circuit in the active balancing circuit bring additional power consumption into the balancing system. To furtherly improve the active balancing performance by reducing the energy loss during the balancing operation, two approaches can be adopted: designing new converter circuit topologies with high efficiency (see Li et al. (2013); Hsieh et al. (2013)) and developing control strategies that minimise the power loss. These two approaches do not contradict each other as the latter one allows to maximise the system performance with the same active balancing circuit and both of them require the understanding of the power loss model of the

⋆ The research was undertaken in collaboration with the WMG Centre High Value Manufacturing Catapult.

balancing circuit. In the work of Baronti et al. (2014), the balancing circuit efficiency has been included in the developed cell balancing models but only fixed and constant energy efficiency is considered. The efficiency and power loss of the dc-dc converters are nonlinear functions of the system states and the system inputs/outputs, the efficiency and power loss do not stay constant when the operating point is changed. Gallardo-Lozano et al. (2014) modelled the power loss as functions of current but the switching loss and the power loss on current ripples are not included. It is necessary to develop a more accurate power loss model to underpin the design of the active balancing control system. In the field of power electronics, the modelling and analysis of the power loss of the dc-dc converters have been investigated by many researchers, but only few research has discussed the topology of ACFC-SR (see Kazimierczuk (2016)). In the work of Xu et al. (2013), the authors discussed the power loss of the ACFC-SR, but the switching loss and the resonating effect of the magnetising current have not been considered, either has the bidirectional operation. Li et al. (2002) developed the ACFC-SR model that includes the resonating magnetising current, the power loss analysis and the bidirectional operation were not investigated.

In this paper, the power loss and efficiency model of the bidirectional ACFC-SR based active balancing circuit are developed. The nonlinear efficiency models of the bidirectional ACFC-SR in charging and discharging mode are developed and involved in the study of the active balancing energy performance. The main contribution of this paper can be summarised as (1) the development of a detailed power loss model for bidirectional ACFC-SR, including the switching loss, the resonating effect, and the bidirectional operation; (2) the performance analysis of the active balancing system with cell-to-external topology (Fig.1); and (3) the optimal balancing current is carried out that can be applied by the active balancing control system to reduce the energy loss during the process of balancing.

2. DYNAMIC MODEL OF THE BIDIRECTIONAL ACFC-SR

The model of the bidirectional ACFC-SR show in Fig.1 is presented in this section. The MOSFET Q_1 works as the main switch whose gate signal is assigned as the control signal, whereas the signals injected to the gates of MOSFETs Q_2 Q_4 are synchronous signals of the control signal. The switching principle of Q_1 Q_4 in normal operation is given as follows: Q_1 and Q_2 are switched complementary, Q_3 should be ON when Q_1 is ON, and Q_4 operates conversely to Q_1.

2.1 Dynamic Equations of the Bidirectional ACFC-SR

To describe the switching behaviour of the ACFC-SR, a switching model is developed and can be written as

$$\begin{cases} L_m \dfrac{di_{Lm}}{dt} = v_1 - (1-S)\, v_{CL} \\ C_{CL} \dfrac{dv_{CL}}{dt} = (1-S)\, i_{Lm} \\ L \dfrac{di_L}{dt} = \dfrac{1}{n} S v_1 - v_2 \end{cases} \tag{1}$$

where S stands for the control signal that controls the main switch Q_1 and i_{Lm} stands for the magnetising current of the transformer, the remaining variables in (1) can be refer to the Fig.1.

Normally, the inductor current i_L is regulated by the converter controller in active balancing applications to obtain desired charging/discharging currents. If a constant switching frequency based inductor current control strategy is applied, the duty cycle of the switching signal S in steady-state, D, can be estimated based on the volt-second balance principle and written as

$$D = n \frac{v_2}{v_1} \tag{2}$$

where n denotes the turns ratio of the transformer. It is noted that the steady-state duty cycle is determined by the transformer turns ratio and the voltage inputs, and is independent of the inductor current.

2.2 Solutions to the Dynamic Equations of the Bidirectional ACFC-SR

Considering the converter operation within one switching period ($0 \le t \le T_s$), the converter actually switches between two linear models according to the status of S. When $S = 1$ ($0 \le t \le dT_s$), the converter dynamic equations can be obtained from (1) as

$$\begin{cases} L_m \dfrac{di_{Lm}}{dt} = v_1 \\ C_{CL} \dfrac{dv_{CL}}{dt} = 0 \\ L \dfrac{di_L}{dt} = \dfrac{1}{n} v_1 - v_2 \end{cases} \tag{3}$$

Solving (2) yields

$$\begin{cases} i_{Lm}(t) = i_{Lm}(0) + \dfrac{v_1}{L_m} t \\ v_{CL}(t) = v_{CL}(0) \\ i_L(t) = i_L(0) + \left(\dfrac{1}{nL} v_1 - \dfrac{1}{L} v_2 \right) t \end{cases} \tag{4}$$

where $i_{Lm}(0)$, $v_{CL}(0)$, and $i_L(0)$ are the initial values of i_{Lm}, v_{CL}, and i_L at $t = 0$, respectively.

When $S = 0$ ($dT_s < t \le T_s$), the differential equations that describe the converter dynamics in this subinterval are given by

$$\begin{cases} L_m \dfrac{di_{Lm}}{dt} = v_1 - v_{CL} \\ C_{CL} \dfrac{dv_{CL}}{dt} = i_{LM} \\ L \dfrac{di_L}{dt} = -v_2 \end{cases} \tag{5}$$

The expressions of i_{Lm}, v_{CL}, and i_L against time can be solved from (5) as

$$\begin{cases} i_{Lm} = A\cos(\omega t) + B\sin(\omega t) \\ v_{CL} = A\xi \sin(\omega t) - B\xi \cos(\omega t) + v_1 \\ i_L(t) = i_L(dT_s) - \dfrac{1}{L} v_2 t \end{cases} \tag{6}$$

where

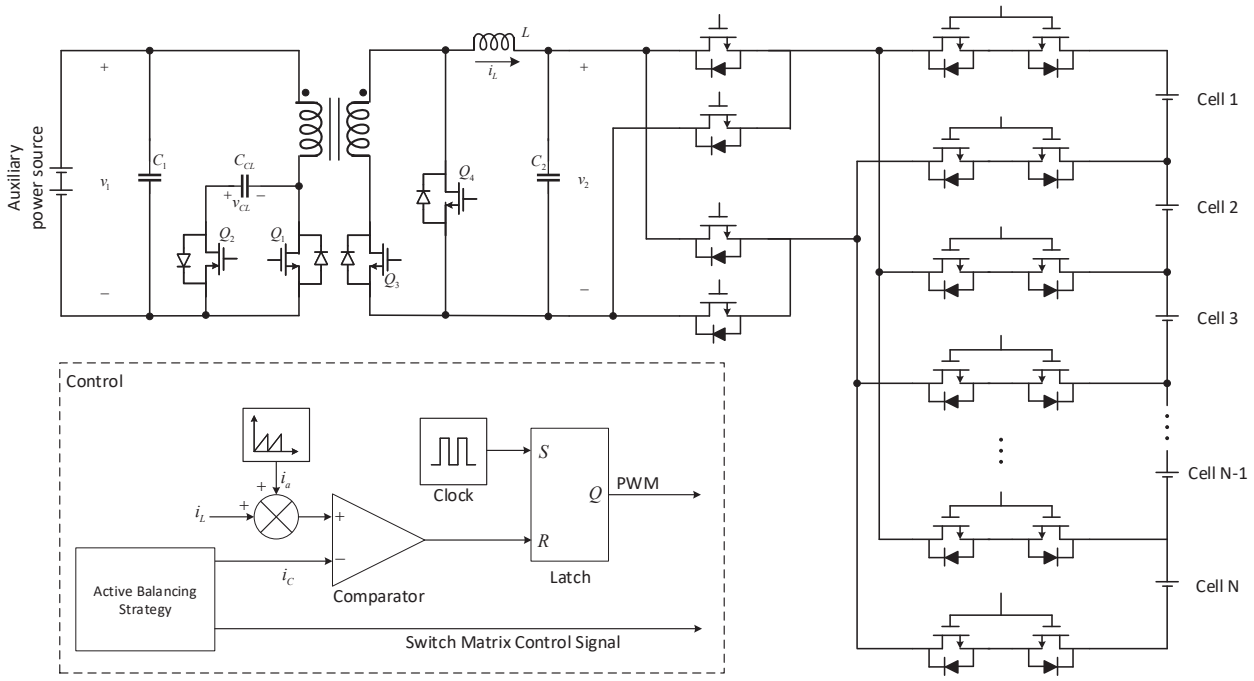

Fig. 1. A bidirectional ACFC-SR based active balancing system

$$\zeta = \sqrt{\frac{L_m}{C_{CL}}}, \omega = \frac{1}{\sqrt{C_{cl} L_m}}, A = i_{Lm}(dT_s)$$
$$B = \frac{1}{\omega L_m}\left[v_1(dT_s) - v_{CL}(dT_s)\right] \quad (7)$$

It is noted that the initial values for solving (5) are determined by the values at the end of the previous subinterval based on the differential equations (3).

Combining (4) and (6), the state variables can be expressed as functions of time, which hold

$$i_{Lm}(t) = \begin{cases} i_{Lm}(0) + \dfrac{v_1}{L_m} t & 0 \le t \le dT_s \\ A\cos(\omega t) + B\sin(\omega t) & dT_s < t \le T_s \end{cases} \quad (8)$$

$$v_{CL}(t) = \begin{cases} v_{CL}(0) & 0 \le t \le dT_s \\ A\xi\sin(\omega t) - B\xi\cos(\omega t) + v_1 & dT_s < t \le T_s \end{cases} \quad (9)$$

$$i_L(t) = \begin{cases} i_L(0) + \left(\dfrac{1}{nL} v_1 - \dfrac{1}{L} v_2\right) t & 0 \le t \le dT_s \\ i_L(dT_s) - \dfrac{1}{L} v_2 t & dT_s < t \le T_s \end{cases} \quad (10)$$

The sinusoidal terms appeared in (8) and (9) in the second subinterval when $S = 0$, represents the resonating effects during the process of transformer reset.

3. EFFICIENCY MODEL OF THE BIDIRECTIONAL ACFC-SR

The converter equivalent circuits with parasitic resistance shown in Fig.2 are studied for the computation of the power loss, including the losses on MOSFET on-resistance R_{Q1} R_{Q4}, transformer winding resistance R_{T1} and R_{T2}, inductance dc resistance R_L, capacitor ESRs R_{CL}, R_{C1} and R_{C2}, current sense resistance R_{S1} and R_{S2}, and the resistance of switching matrix and writing R_2. Additionally, the transformer core loss and MOSFET switching loss are also included in the total power loss.

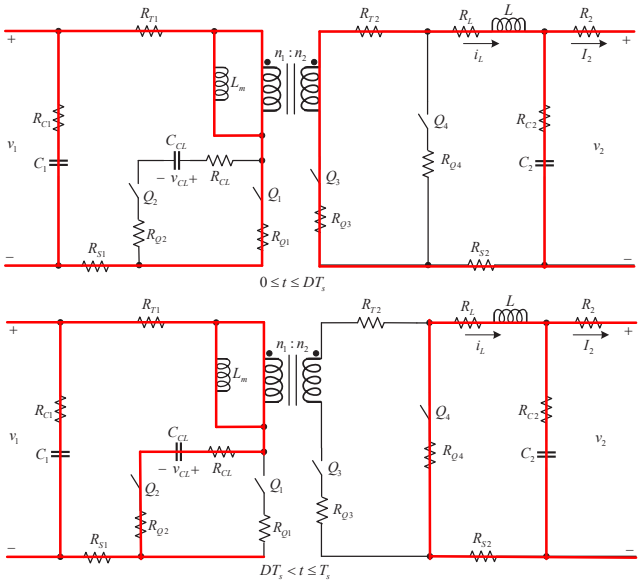

Fig. 2. Equivalent circuits of the bidirectional ACFC-SR with parasitic resistances in steady-state

The efficiency model of the bidirectional ACFC-SR are developed based on the following assumptions: (1) the converter is operating in steady-state; (2) the dead-time of switching devices is ignored; (3) the filtering capacitor C_1 and C_2 is designed to perfectly filter the current ripple, so the input and output currents are equal to the dc component of the primary winding current and the inductor current, respectively. (4) the MOSFET output capacitance is linear. (5) the terminal voltages, v_1 and v_2, are constant over one switching period.

Based on the above assumption, the initial values of $i_L(t)$ for the first and the second subintervals in steady state can be obtained as

$$i_L(0) = I_L - \frac{v_2 T_s}{2L}\left(1 - n\frac{v_2}{v_1}\right) \tag{11}$$

$$i_L(DT_s) = I_L + \frac{v_2 T_s}{2L}\left(1 - n\frac{v_2}{v_1}\right) \tag{12}$$

where I_L is the dc component of the inductor current that is equal to the output current I_2, which is the charging/discharging current that is regulated by the active balancing controller. To simplify the calculation process, the initial values of the magnetising current and the active clamp capacitor voltage are approximated by

$$i_{Lm}(0) = 0, i_{Lm}(DT_s) = n\frac{v_2 T_s}{L_m}, v_{CL}(0) = v_{CL}(DT_s) = v_1 \tag{13}$$

3.1 MOSFET Power Loss

The power loss of the MOSFETs consists of the conduction loss and the switching loss. For the MOSFET conduction loss, the currents passing through - over one switching period need to be figured out to estimate the conduction loss on R_{Q1} - R_{Q4}.

Conduction loss on R_{Q1}. The current passing though $Q1$ over one switching period is

$$i_{Q1} = \begin{cases} \frac{1}{n} i_L + i_{Lm} & 0 < t \le DT_s \\ 0 & DT_s < t \le T_s \end{cases} \tag{14}$$

Substituting (8), (10), and (11)-(13) into (14) yields

$$i_{Q1} = \begin{cases} \frac{1}{n}(I_L - M) + \left(\frac{\Pi}{n} + \frac{v_1}{L_m}\right) t & 0 < t \le D_{Q1} T_s \\ 0 & D_{Q1} T_s < t \le T_s \end{cases} \tag{15}$$

where

$$M = \frac{v_2 T_s}{2L}\left(1 - n\frac{v_2}{v_1}\right), \Pi = \frac{1}{nL} v_1 - \frac{1}{L} v_2 \tag{16}$$

The rms value of i_{Q1} is

$$i_{Q1rms} = \sqrt{\frac{1}{T_s}\int_0^{DT_s} i_{Q1}^2 dt} = \sqrt{\frac{1}{n^2}(I_L - M)^2 D} \\ + \frac{1}{3}\left(\frac{\Pi}{n} + \frac{v_1}{L_m}\right)^2 D^3 T_s^2 + \frac{1}{n}(I_L - M)\left(\frac{\Pi}{n} + \frac{v_1}{L_m}\right) D^2 T_s \tag{17}$$

Then the power loss due to R_{Q1} can be calculated by

$$P_{Q1} = R_{Q1} i_{Q1rms}^2 \tag{18}$$

Conduction loss on R_{Q2}. The MOSFET Q_2 conducts during the time interval $DT_s < t \le T_s$ so the current passing Q_2 over one switching period is

$$i_{Q2} = \begin{cases} 0 & 0 \le t \le DT_s \\ i_{Lm} & DT_s < t \le T_s \end{cases} \tag{19}$$

Its rms value is calculated by

$$i_{Q2rms} = \sqrt{\frac{1}{T_s}\int_0^{(1-D)T_s} i_{Q2}^2 dt} \\ = \sqrt{\left[\frac{A^2}{4\omega T_s}\sin(2\omega(1-D)T_s) + \frac{A^2}{2}(1-D)\right]} \tag{20}$$

Then the power loss on R_{Q2} is

$$P_{Q2} = R_{Q2} i_{Q2rms}^2 \tag{21}$$

Conduction loss on R_{Q3}. The expression of the current passing through Q_3 is

$$i_{Q3} = \begin{cases} i_L & 0 \le t \le DT_s \\ 0 & DT_s < t \le T_s \end{cases} \tag{22}$$

Its rms value is

$$i_{Q3rms} = \sqrt{\frac{1}{T_s}\int_0^{DT_s} i_{Q3}^2 dt} \\ = \sqrt{\frac{1}{3}\Pi^2 D^3 T_s^2 + (I_L - M)^2 D + (I_L - M)\Pi D^2 T_s} \tag{23}$$

So the power loss on R_{Q3} is

$$P_{Q3} = R_{Q3} i_{Q3rms}^2 \tag{24}$$

Conduction loss on R_{Q4}. The current passing Q_4 is

$$i_{Q4} = \begin{cases} 0 \ for & 0 \le t \le DT_s \\ i_L \ for & DT_s < t \le T_s \end{cases} \tag{25}$$

and its rms value

$$i_{Q4rms} = \sqrt{\frac{1}{T_s}\int_0^{(1-D)T_s} i_{Q4}^2 dt} = \sqrt{(I_L + M)^2 (1-D)} \\ + \frac{v_2^2}{3L^2}(1-D)^3 T_s^2 - (I_L + M)\frac{v_2}{L}(1-D)^2 T_s} \tag{26}$$

Hence, the power loss on R_{Q4} is

$$P_{Q4} = R_{Q4} i_{Q4rms}^2 \tag{27}$$

MOSFET switching loss. The switching loss of a MOSFET, including both switching –ON and –OFF loss, can be approximated using the equation

$$P_{sw} = f_s C_0 V_{DS}^2 \tag{28}$$

where C_0 is linear output capacitance of the MOSFET, V_{DS} is the drain-to-source voltage in off-state, and f_s is the switching frequency.

3.2 Forward Transformer Power Loss

The power loss of the forward transformer is modelled by the sum of the conduction loss on R_{T1}, R_{T2} and the transformer core loss. The current passing through R_{T1} can be expressed as

$$i_{T1} = \begin{cases} i_{Q1} & 0 < t \le DT_s \\ i_{Q2} & DT_s < t \le T_s \end{cases} \tag{29}$$

where and can be obtained from (15) and (19). The rms value of i_{T1} can be calculated by

$$i_{T1rms} = \sqrt{\frac{1}{T_s}\left(\int_0^{DT_s} i_{Q1}^2 dt + \int_0^{(1-D)T_s} i_{Q2}^2 dt\right)} = \sqrt{i_{Q1rms}^2 + i_{Q2rms}^2} \quad (30)$$

The values of and are available from (17) and (20), respectively. So, the power loss on R_{T1} is

$$P_{T1} = R_{T1} i_{T1rms}^2 = R_{T1}\left(i_{Q1rms}^2 + i_{Q2rms}^2\right) \quad (31)$$

Since R_{T2} is in series of R_{Q3}, the current i_{Q3} also passes through R_{T2}. Thus, the power loss on R_{T2} can be calculated by

$$P_{T2} = R_{T2} i_{Q3rms}^2 \quad (32)$$

The transfer core loss cannot be ignored when operating with a high frequency. To estimate the core loss, the following equation is used

$$P_{core} = \alpha {f_s}^{1.63} \Delta B^{2.63} \quad (33)$$

where is a loss coefficient and ΔB can be obtained by

$$\Delta B = K_1 V_T T \quad (34)$$

in which K_1 is a loss coefficient, V_T is the transformer terminal voltage, T is the time that V_T is applied during one switching period.

3.3 Other Conduction Loss

Other conduction loss of the converter contains the loss on the current sense resistors, the capacitor ESRs, inductor resistance, and the switching matrix and wiring conduction loss. The calculations of those conduction losses are explained as follows.

Power loss on the inductor. The inductor current over one switching period can be obtained as

$$i_L = \begin{cases} i_{Q3} & 0 < t \le DT_s \\ i_{Q4} & DT_s < t \le T_s \end{cases} \quad (35)$$

and its rms value

$$i_{Lrms} = \sqrt{\frac{1}{T_s}\left(\int_0^{DT_s} i_{Q3}^2 dt + \int_0^{(1-D)T_s} i_{Q4}^2 dt\right)} = \sqrt{i_{Q3rms}^2 + i_{Q4rms}^2} \quad (36)$$

Hence the power loss on R_L is

$$P_L = R_L\left(i_{Q3rms}^2 + i_{Q4rms}^2\right) \quad (37)$$

Power loss on current sense resistors. It is shown in Fig.2 that R_{S1} is in series with R_{T1} whereas R_{S2} and R_L are in series such that the currents passing R_{S1} and R_{S2} are identical to the currents i_{T1} and i_L, respectively. It is straightforward to obtain the power loss on R_{S1} and R_{S2} using (30) and (36) as

$$P_{S1} = R_{S1}\left(i_{Q1rms}^2 + i_{Q2rms}^2\right) \quad (38)$$

$$P_{S2} = R_{S2}\left(i_{Q3rms}^2 + i_{Q4rms}^2\right) \quad (39)$$

Power loss on capacitor ESRs. Base on the assumption that the filtering capacitors C_1 and C_2 can fully cancel the current ripple, the current passing through R_{C1} is

$$i_{C1} = \begin{cases} -\frac{1}{n}M + \left(\frac{\Pi}{n} + \frac{v_1}{L_m}\right)t & 0 < t \le DT_s \\ i_{Q2} & DT_s < t \le T_s \end{cases} \quad (40)$$

and the current passing through R_{C2} is

$$i_{C2} = i_L - I_L = \begin{cases} -M + \Pi t & 0 \le t \le DT_s \\ M - \frac{1}{L}v_2 t & DT_s < t \le T_s \end{cases} \quad (41)$$

Calculating the rms of (40) and (41) yields

$$i_{C1rms} = \sqrt{\frac{1}{n^2}M^2 D + \frac{1}{3}\left(\frac{\Pi}{n} + \frac{v_1}{L_m}\right)^2 D^3 T_s^2 - \frac{M}{n}\left(\frac{\Pi}{n} + \frac{v_1}{L_m}\right)D^2 T_s + i_{Q2rms}^2} \quad (42)$$

and

$$i_{C2rms} = \sqrt{\frac{1}{3}\Pi^2 D^3 T_s^2 - M\Pi D^2 T_s + \frac{v_2^2}{3L^2}(1-D)^3 T_s^2 - \frac{v_2}{L}M(1-D)^2 T_s + M^2} \quad (43)$$

Therefore, the power loss on and can be calculated by

$$P_{C1} = R_{C1} i_{C1rms}^2, P_{C2} = R_{C2} i_{C2rms}^2 \quad (44)$$

With respect to R_{CL} , which is in series with R_{Q3}, its current is equal to i_{Q2} so the power loss on R_{CL} can be obtained by

$$P_{CL} = R_{CL} i_{Q2rms}^2 \quad (45)$$

Power loss on switching matrix and wiring. The current passing through R_2 is equivalent to the balancing current that charges/discharges a cell. With the assumption that the balancing current equals to the dc component of the inductor current, there is

$$I_2 = I_L \quad (46)$$

Then the power loss on R_2 can be calculated by

$$P_2 = R_2 I_L^2 \quad (47)$$

The Efficiency of the Bidirectional ACFC-SR. The total power loss of the bidirectional ACFC-SR can be obtained by adding up all power loss calculated in previous sections:

$$\begin{aligned} P_{Loss} = {} & P_{Q1} + P_{Q2} + P_{Q3} + P_{Q4} + P_{T1} + P_{T2} \\ & + P_{C1} + P_{C2} + P_L + P_{core} + P_{CL} + P_{sw1} \\ & + P_{sw2} + P_{sw3} + P_{sw4} + P_2 + P_{Supply} \end{aligned} \quad (48)$$

where P_{Supply} stands for the power consumption for the electronic system such as the MOSFET driver, monitoring and protection ICs, and communication modules etc. It should be noted that the derived total converter power loss, P_{Loss}, is the function of the terminal voltage, v_1 and v_2, and the system output I_L. As the converter dynamics are much faster than the dynamics of the battery cells, the voltage inputs of the converter can be considered to be constant during a short period of operating. Under this circumstance, the power loss is mainly determined by the dc component of the inductance current, I_L, which is the balancing current determined by the high-level controller.

When the converter is operating in charging mode with charging current $I_L > 0$, the efficiency can be calculated by

$$\eta_c = \frac{|v_2 I_L|}{|v_2 I_L| + P_{Loss}} \tag{49}$$

When the converter is operating in discharging mode with charging current $I_L < 0$, the efficiency can be calculated by

$$\eta_d = \frac{|v_2 I_L| - P_{Loss}}{|v_2 I_L|} \tag{50}$$

4. ACTIVE BALANCING ENERGY LOSS MODEL

The energy loss model of the active balancing system with the circuit topology shown in Fig.1 is developed for the investigation of energy loss during the active balancing process. The nonlinear efficiency models (49) and (50) are integrated. The approach presented in the work of Baronti et al. (2014) is used.

Define $N \in \mathbb{Z}$ as the number of cells connected in series and Q_i ($i \in [1 \dots N]$) as the charges stored in cell i before the start of balancing. It is assumed that the cells are sorted in a charge-descending order, namely $Q_1 \geq Q_2 \geq \dots \geq Q_N$. Assuming that all cells reach the same charge level after balancing, the final amount of charges in each cell when balancing is completed is defined as Q_F. The implementation of active balancing with topology in Fig.1 requires transferring charges from 'strong' cells to the external power storage device via the discharging process and then moving those charges to the 'weak' cells via the charging process. Defining $M \in [1 \dots N]$ the number of 'strong' cells, it holds

$$\eta_d \sum_{i=1}^{M} (Q_i - Q_F) = \frac{1}{\eta_c} \sum_{i=M+1}^{N} (Q_F - Q_i) \tag{51}$$

Solving (51) for Q_F yields

$$Q_F = \frac{\eta_d \eta_c \sum_{i=1}^{M} Q_i + \sum_{i=M+1}^{N} Q_i}{N - (1 - \eta_d \eta_c) M} \tag{52}$$

It can be observed that when there is not power loss on the balancing circuit, the final charge amount of each cell equals to the average charges before balancing, thus the value of M should be chosen such that

$$Q_{avg} \geq Q_F > Q_{M+1} \tag{53}$$

The total balancing time can be obtained by the sum of charging mode time and discharging mode time, which holds

$$T = T_d + T_c = \frac{\sum_{i=1}^{M} (Q_i - Q_F)}{I_{bal\_d}} + \frac{\sum_{i=M+1}^{N} (Q_F - Q_i)}{I_{bal\_c}} \tag{54}$$

where T_d is the total discharging time, T_c is the total charging time, I_{bal_d} is the balancing current during discharging process, and I_{bal_c} is the balancing current during charging process.

In simple rule-based active balancing control, the charging and discharging balancing current are chosen to be the same. In this case, there is

$$I_{bal\_c} = I_{bal\_d} = I_{bal} = |I_L| \tag{55}$$

Then, the expression of (**??**) can be rearranged and simplified as

$$T = \frac{1}{|I_L|} \left(\frac{1}{\eta_c \eta_d} + 1 \right) \sum_{i=M+1}^{N} (Q_F - Q_i) \tag{56}$$

The energy loss due to the balancing process can be estimated according to (48) and (54) by

$$E_{Loss} = T_d P_{Loss}(I_L) + T_c P_{Loss}(-I_L) \tag{57}$$

5. CASE STUDY

The energy loss and balancing time of an active balancing system containing 5 cells in series with the balancing circuit in Fig.1 is studied in this section via Matlab. The 5 cells are assumed to be identical to each other but with different initial SOCs. The capacity of each cell is $5Ah$ and the initial SOCs for cell 1–5 are given in descending order as 80%, 77%, 44%, 38%, and 20% respectively, which are generated randomly. With initial SOCs, the charge amount in every single cell can be obtained as $14400As$, $13860As$, $7920As$, $6840As$, $3600As$. The small variation of the cell terminal voltage is ignored, and the terminal voltage for each cell is $3.6V$. The terminal voltage of the external power supply is $12V$. The parameters of the active balancing system are provided in the Appendix.

5.1 Balancing Circuit Efficiency

The converter efficiency and power loss in both charging and discharging mode are plotted in Fig.3(a) and Fig.3(b) respectively. It can be seen in Fig.3(a) that the power efficiencies in charging mode and discharging mode are different. The efficiencies in charging mode are higher than in discharging mode. The maximum efficiencies can be found at $I_L = 0.88A$ for both charging and discharging mode, which are 87.46% and 85.80%, respectively. The efficiency difference between charging and discharging mode would increase if the balancing current is further away from the maximum point. Although Fig.3(a) indicates different efficiency curves in charging and discharging mode, Fig.3(b) shows that the power loss in the discharging mode are identical to the power loss in the charging mode. The power loss would increase with increased balancing current, the smaller balancing current would result in a lower loss power.

5.2 Active Balancing Performance

The required balancing time and the energy loss on the balancing circuit against balancing current are shown in Fig.4(a) and Fig.4(b), respectively. Fig.4(a) indicates that the balancing time would reduce with the increase of the balancing current. When balancing current increases from $0A$ to $1A$, a significant improvement in balancing time can be observed, whereas the balancing time reduces slower when increasing the balancing current from $1A$ to $5A$.

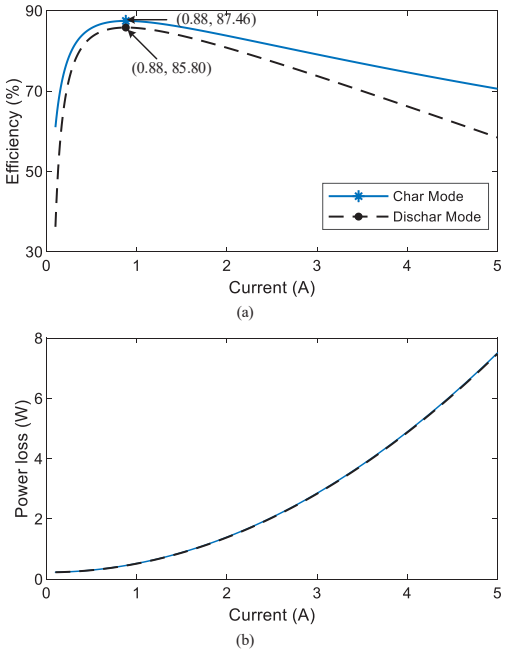

Fig. 3. Converter efficiency and power loss with different balancing current: (a) converter efficiency versus current, (b) power loss versus current

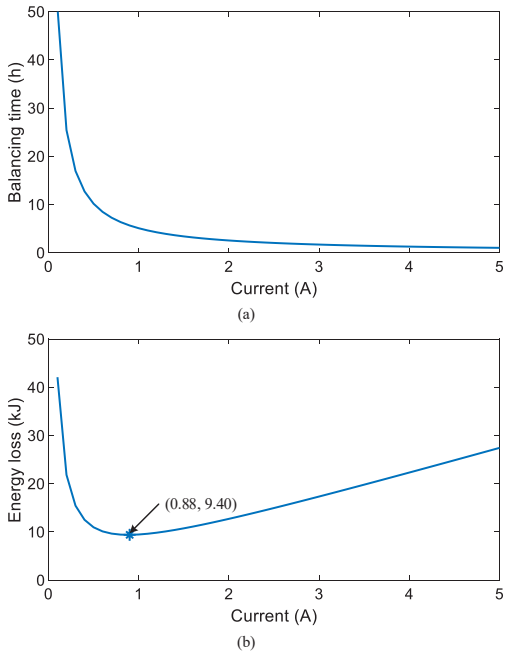

Fig. 4. Relationship between the energy loss, the balancing time, and the balancing current: (a) balancing time versus balancing current, (b) power loss versus balancing current

Although the larger balancing current results in a higher power loss (see Fig.3(b)), the loss of energy may not be monotonically increasing with the increase of balancing current, which is indicated in Fig.4(b). This is because the high balancing current could shorten the balancing time, which may relieve the effects of power loss increasing. The minimum point of energy loss ($9.40kJ$) can be found at $I_L = 0.88A$, which would be the optimal balancing current if the objective is to minimise the energy loss during the balancing process. It should be noted that this optimal point is also the point at which the converter has the maximum power efficiency.

The relationship between the energy loss and the balancing current is depicted Fig.5. It can be seen that when the minimum energy loss over the balancing period is achieved, the required balancing time needed is 5.65 hours. There is a trade-off between the low energy loss and the fast balancing time as the balancing time faster than this minimum-loss point would cause an increase of the energy loss.

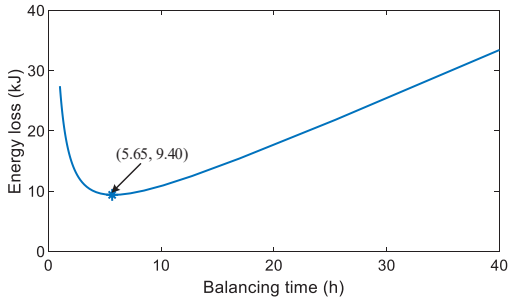

Fig. 5. Relationship between the balancing time and the energy loss

6. CONCLUSION

The energy loss and efficiency models for the bidirectional ACFC-SR based active balancing system has been developed in this paper. The derived power loss model of the directional ACFC-SR has included the MOSFET switching loss, transformer core loss, and the resonating effect of the transformer magnetising current. The efficiency model for both charging and discharging operations of the balancing system has been derived. It has been shown that the efficiency of the active balancing system is a nonlinear function of the converter terminal voltages and the balancing current. The optimal balancing current can then be obtained with which the balancing system could operate at the maximum efficiency point to get the minimum energy loss.

REFERENCES

Baronti, F., Roncella, R., and Saletti, R. (2014). Performance comparison of active balancing techniques for lithium-ion batteries. *Journal of Power Sources*, 267, 603 – 609. doi: https://doi.org/10.1016/j.jpowsour.2014.05.007.

Cordoba-Arenas, A., Onori, S., and Rizzoni, G. (2015). A control-oriented lithium-ion battery pack model for plug-in hybrid electric vehicle cycle-life studies and system design with consideration of health management. *Journal of Power Sources*, 279, 791 – 808. 9th Inter-

national Conference on Lead-Acid Batteries – LABAT 2014.

Daowd, M., Omar, N., Van Den Bossche, P., and Van Mierlo, J. (2011). Passive and active battery balancing comparison based on matlab simulation. In *2011 IEEE Vehicle Power and Propulsion Conference*, 1–7. doi: 10.1109/VPPC.2011.6043010.

Daowd, M., Omar, N., Van den Bossche, P., and Van Mierlo, J. (2011). A review of passive and active battery balancing based on matlab/simulink. *Journal of International Review of Electrical Engineering (IREE)*, 6, 2974–2989.

Gallardo-Lozano, J., Romero-Cadaval, E., Milanes-Montero, M.I., and Guerrero-Martinez, M.A. (2014). Battery equalization active methods. *Journal of Power Sources*, 246, 934 – 949. doi: https://doi.org/10.1016/j.jpowsour.2013.08.026.

Hannan, M.A., Hoque, M.M., Ker, P.J., Begum, R.A., and Mohamed, A. (2017). Charge equalization controller algorithm for series-connected lithium-ion battery storage systems: Modeling and applications. *Energies*, 10(9). doi:10.3390/en10091390.

Hsieh, Y., Liang, T., Chen, S.O., Horng, W., and Chung, Y. (2013). A novel high-efficiency compact-size low-cost balancing method for series-connected battery applications. *IEEE Transactions on Power Electronics*, 28(12), 5927–5939. doi:10.1109/TPEL.2013.2246584.

Kazimierczuk, M.K. (2016). *Pulse-Width Modulated DC-DC Power Converters, 2nd Edition*. Wiley.

Kutkut, N.H. and Divan, D.M. (1996). Dynamic equalization techniques for series battery stacks. In *Proceedings of Intelec'96 - International Telecommunications Energy Conference*, 514–521. doi: 10.1109/INTLEC.1996.573384.

Lee, K., Chung, Y., Sung, C., and Kang, B. (2015). Active cell balancing of li-ion batteries using *lc* series resonant circuit. *IEEE Transactions on Industrial Electronics*, 62(9), 5491–5501. doi:10.1109/TIE.2015.2408573.

Li, Q.M., Lee, F.C., and Jovanovic, M.M. (2002). Large-signal transient analysis of forward converter with active-clamp reset. *IEEE Transactions on Power Electronics*, 17(1), 15–24. doi:10.1109/63.988664.

Li, S., Mi, C.C., and Zhang, M. (2013). A high-efficiency active battery-balancing circuit using multiwinding transformer. *IEEE Transactions on Industry Applications*, 49(1), 198–207. doi:10.1109/TIA.2012.2229455.

Xu, S., Zhang, T., Yao, Y., and Sun, W. (2013). Power loss analysis of active clamp forward converter in continuous conduction mode and discontinuous conduction mode operating modes. *IET Power Electronics*, 6(6), 1142–1150. doi:10.1049/iet-pel.2013.0019.

Appendix A. SYSTEM PARAMETERS IN CASE STUDY

$n = 1.14$
$R_1 = 17.6m\Omega, R_2 = 31.6m\Omega, L_m = 112.15\mu H$
$L = 6.8\mu H, R_L = 8.98m\Omega, C_2 = 9.9\mu F, R_{C2} = 4.76m\Omega$
$C_1 = 9.4\mu F, R_{C1} = 3m\Omega, C_{CL} = 0.022\mu F, R_{CL} = 1m\Omega$
$R_{Q1} = R_{Q2} = 0.041m\Omega, R_{Q3} = R_{Q4} = 4.4m\Omega$
$C_{0\_Q1} = C_{0\_Q2} = 600pF, C_{0\_Q3} = C_{0\_Q4} = 812pF$
$R_{sense} = 0.01\Omega$